Annihilation Density Distribution Calculations for Medically Important Positron Emitters

Matthew R. Palmer, *Member, IEEE*, and Gordon L. Brownell

Abstract— The effect of positron range on the image-plane resolution of tomographic images is evaluated through calculations based on a model which employs beta-decay energy spectra and an empirical range formula. Predicted range distribution functions are compared with published measurements for three medically important positron emitters; ^{11}C, ^{68}Ga, and ^{82}Rb. The effect of tomographic slice thickness on point-source annihilation distribution functions is also demonstrated. Line-spread functions are calculated using the model, for the above isotopes as well as for ^{18}F, ^{15}O, and ^{13}N. Image-plane resolution predictions are made for high-resolution positron cameras for various positron emitting isotopes with end-point energies up to 4 Mev.

I. INTRODUCTION

THE spatial resolution of positron emission tomography (PET) cameras has steadily improved over the past few years. Cerebral studies in man are now possible with an in-plane spatial resolution of better than 5 mm full-width at half-maximum (FWHM) [1], [2]. A central question for high-resolution PET studies, is that of the fundamental limits of imaging with positrons—the positron range and the deviation of annihilation gamma rays from 180 degrees. The latter has been well characterized [3], but the effects of positron range are not so well understood. The resolution of tomographic instruments is approaching these fundamental limits, generating renewed interest in positron range effects and the possibility of reducing them through instrument design or image postprocessing [4], [5].

Positron range measurements have been attempted for a number of emitters by several groups [6]–[8]. The considerable variation in experimental results has lead to some controversy over the magnitude of this effect. Of the published measurements to date, Derenzo's work appears to be the most accurate, and that which is likely to reduce the systematic errors introduced by detector limitations [7], [5]. He has found that annihilation density distributions, projected onto the sinogram axis, arising from near-point sources are well approximated by a bi-exponential model. Approximate model parameters have been published for the medically-important isotopes of ^{18}F, ^{11}C, ^{68}Ga, and ^{82}Rb. While these estimated model parameters are adequate for certain predictions, the central issue of the extent and nature of image-plane resolution loss due to positron range blurring has yet to be fully

resolved. In addition, Derenzo's experimental technique is not well suited to the measurement of range distributions from nongenerator produced, short-lived isotopes such as ^{13}N and ^{15}O, and so positron range effects are difficult to assess for these isotopes.

Since the Derenzo publication in 1979, little attention has been directed towards the issue of positron range and its effect on the spatial resolution of PET imagery. As the resolution of positron cameras improves, the resolution limits imposed by positron range will become a significant fraction of the overall systematic error associate with PET measurements. The goal of this work is to develop a model which will predict the effects of positron range in terms of physical parameters. In this way, the data may be applied to evaluate competing designs for new tomographs and to evaluate proposed schemes that attempt to correct PET measurements for positron range effects.

II. MODEL DEVELOPMENT

Consider an isotropically radiating point source of monoenergetic positrons located at the origin of a three-dimensional absorber. For positrons with relatively low end-point energies interacting with materials that have low atomic numbers (relevant in the current study; end-point energy, $E_0 < 4$ MeV, and atomic number, $Z \approx 7$) the predominant mode of energy loss is through ionization and excitation of atomic electrons since the Bremsstrahlung loss is very small [9]. A positron typically interacts with a great number of electrons before reaching thermal energy [10, pp. 268–275]. A positron trajectory is tortuous and, following a small number of collisions which could involve large scattering angles, the particle's direction and position is nearly independent of its initial direction of motion. Under these conditions, in order to simplify the analysis, we treat the problem as though the positrons behave diffusively (see Evans [11, pp. 627–629] for a discussion that supports this argument). With this assumption, we expect the equilibrium particle density resulting from a point source application of monoenergetic positrons to be represented by a three-dimensional Gaussian distribution centered at the origin. Furthermore, the energy spectrum for particles after traversal through an absorber, is approximately independent of the absorber thickness (see Evans [11, p. 629], and so we assume that the ratio of particle density to annihilation density is approximately constant. The three dimensional annihilation density is therefore approximated by

$$D_m(r; E_i) \approx \frac{1}{\left(\sqrt{2\pi}\sigma\right)^3} e^{-r^2/2\sigma^2} \qquad (1)$$

where r is the radial distance from the origin and $\sigma = \sigma(E_i)$ is the standard deviation, a function of the initial energy E_i.

Providing we can find an expression which relates the monoenergetic distribution parameter σ to the emission energy, the annihilation density for a point-source beta emitter in an infinite isotropic medium is given by

$$D(r) = \int_0^{E_0} D_m(r; E_i) N(E_i)\, dE_i \qquad (2)$$

where the energy spectrum is denoted $N(E_i)$, and represents the probability that a particle's initial energy lies in the interval $(E_i, E_i + dE_i)$ [11, pp. 548–554], and E_0 is the beta endpoint energy.

A. Range-Energy Relationship

Tabata, Iot, and Okabe have determined a semi-empirical expression that relates electron range and initial energy by considering experimental results available prior to 1972 [12]. In these experiments, a collimated beam of monoenergetic electrons is directed at a slab of test material. A detector located beyond the exit surface of the slab measures the intensity of the emerging beam. The slab thickness is varied, and a curve of transmitted fraction versus slab thickness is thus produced. The extraprolated range R_{ex} is measured from the curve by extrapolating the linear portion of the curve to the background. The expression for R_{ex}, valid for electrons with initial energies in the 300 eV to 30 MeV range, is a function of incident electron energy and the effective atomic number and atomic weight of the stopping material.

Values for the effective atomic weight and atomic number for water are $A_w = 13.0$ and $Z_w = 7.22$, and for polyurethane, $A_p = 12.2$ and $Z_p = 6.51$ (calculations are based on formulas given in [13, pp. 130–131]). These two materials have relatively low atomic number and therefore the expression for R_{ex} very much simplifies to

$$R_{\text{ex}}(E_i) \approx \frac{b_1 E_i^2}{b_2 + E_i} \qquad (3)$$

where R_{ex} is expressed in mm, and with incident energy E_i expressed in MeV. The empirical constants are defined as

$$b_1 = \frac{4.569A}{Z^{1.209}} \quad b_2 = \frac{1}{2.873 - 0.02309Z}. \qquad (4)$$

To a first approximation, we expect this equation to be valid for positrons since the stopping power of a material is approximately the same for electrons and positrons.[1] We can apply the foregoing assumptions to the geometry of the electron beam transmission experiment by taking the point at which the beam hits the test slab as the coordinate system origin. At the exist surface of the test slab a detector records the intensity of the emerging beam, weighted according to the detector's aperture function. Following the above analysis, we assume

that the intensity of the emerging beam is representative of the annihilation density at the surface of the slab. Since we are dealing with a three-dimensional Gaussian distribution, summation over a plane surface, weighted by the detector aperture function results in a one-dimensional Gaussian transmission curve, provided that the detector aperture function is also approximately Gaussian in form. Furthermore, the standard deviation of the transmission curve is the same as that of the original three-dimensional annihilation density distribution. If we draw a line tangent to the Gaussian shaped transmission curve, at the point of maximum slope it will intersect the range axis at twice the standard deviation. That is, the relationship between initial energy and distribution parameter σ is approximated by

$$\sigma(E_i) \approx R_{\text{ex}}(E_i)/2 \qquad (5)$$

where E_i is the initial energy and R_{ex} is the extrapolated range, defined in (3).

III. MODEL VALIDATION

The experimental results presented by Derenzo [7], [5] were obtained with the Donner 280-Crystal tomograph using small sources of positron emitter placed inside polyurethane foam cylinders. The tomograph's in-plane resolution and slice thickness were both reported to be 7.5 mm FWHM. Point-spread functions (PSF) were presented for ^{11}C, ^{68}Ga, [82]Rb [7] and then later for [18]F [5]. For the purpose of comparing model predictions and experimental results, we have chosen to work only with the isotopes for which raw data were presented (^{11}C, ^{68}Ga, and [82]Rb) since we are not confident in the accuracy of the postprocessing schemes nor the exact form of the suggested model.[2]

In order to obtain an expression for projected annihilation density functions suitable for comparison with experimental results, (2) must be manipulated, first by taking a *weighted* Abel transform in the axial direction, followed by an Abel transform (see Appendix) to project the distribution onto the sinogram axis. The weighted Abel transform is taken with a standard deviation corresponding to the tomograph resolution in the axial direction, σ_t. The two-dimensional axial-plane, or image-plane, annihilation density distribution is given by

$$Q(\rho) = \int_{-\infty}^{\infty} D\left(\sqrt{\rho^2 + z^2}\right) e^{-z^2/2\sigma_t^2}\, dz$$

$$= \mathcal{A}_{\sigma_t}\{D(r); \rho\} \qquad (6)$$

where ρ is the radial distance in the axial plane. The one-dimensional projected annihilation density distribution is given

---

[1] We expect the difference in stopping power to be less than about 5% in the energy range of interest here. For higher end-point energy emitters such as [82]Rb, the difference may be greater than this (see, for example, [14]) which may be a factor contributing to the higher discrepancy between model generated predictions and published measurements that we observe for [82]Rb.

[2] In order to isolate positron range effects, Derenzo repeated the experiment with the sources enclosed in aluminum casings. The intent was to measure the blurring due to other systematic effects (source size, detector size, and angular deviation of annihilation gamma rays) and then deconvolve the measured data for these effects. Problems exist with this data because of gross undersampling, and because at least for ^{11}C, the projected PSF exhibits sharper resolution than a theoretical point source in this machine.
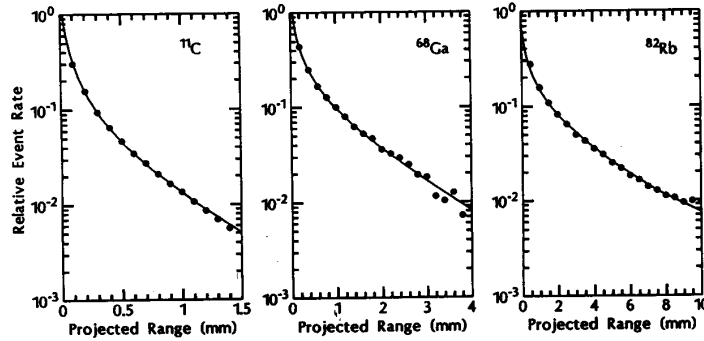
Fig. 1. Comparison of model predictions (smooth curves) and Derenzo's experimental results (dots) for projected annihilation density distributions due to point sources of positron emitting isotopes.

by

$$P(u) = \int\limits_{-\infty}^{\infty} Q\left(\sqrt{u^2 + t^2}\right) dt$$

$$= \mathcal{A}\{Q(\rho); u\} = \mathcal{A}\{\mathcal{A}_{\sigma_t}\{D(r); \rho\}; u\} \qquad (7)$$

where u is the displacement from the sinogram-axis origin. Because of the linearity properties of these two transformations, we can evaluate the two Abel integrals directly on the monoenergetic kernel of (1), and then rewrite (2) in the sinogram-domain as

$$P(u) = \int\limits_{0}^{E_0} P_m(u; E_i) N(E_i) \, dE_i \qquad (8)$$

where the projected mono-energetic kernel P_m is given by

$$P_m(u; E_i) = \frac{\sigma_t}{\sqrt{2\pi}\sigma\sigma_f} e^{-u^2/2\sigma^2} \qquad (9)$$

and where we have introduced σ_f, the effective standard deviation, which is given by

$$\sigma_f = \sqrt{\sigma^2 + \sigma_t^2}. \qquad (10)$$

Numerical integration was performed according to (8) to produce projected positron range distributions for the three isotopes for which raw experimental data were available; ^{11}C, ^{68}Ga, and ^{82}Rb. The resulting curves are shown overlaid with Derenzo's measured results in Fig. 1. In each case, the model-generated curve matches the experimental data very closely. It should be emphasized here that the model was not *fit* to the data (except for an offset adjustment, performed visually, which corresponds to a single arbitrary normalization factor) since there are no free parameters. The value used for σ_t corresponds to the reported slice thickness of 7.5 mm FWHM [7] and the function $R_{ex}(E_i)$, which determines σ, was calculated according to (3) and (4), using the effective atomic weight and atomic number of polyurethane given previously. Both these parameters were scaled according to the density of the polyurethane foam used in each of Derenzo's measurements

A. Effect of Slice Thickness

A limitation to the general usefulness of Derenzo's experimental results and his empirical model for projected annihilation density distributions is due to the tomograph's limited resolution in the axial direction, or slice "thickness." It is possible however, to correct the data (or at least the empirical model expressions) to remove the effect of slice thickness. Expressing (6) as an inverse weighted Abel transform, we have

$$D(r) = \mathcal{A}_{\sigma_t}^{-1}\{Q(\rho); r\} \qquad (11)$$

and then employing (A-7) from the Appendix, we obtain

$$D(r) = \frac{-1}{2\pi}\mathcal{A}_{\sigma_t}\left\{\frac{1}{\sigma_t^2}Q(\rho) - Q'(\rho)/\rho; r\right\}. \qquad (12)$$

Sampling the three-dimensional distribution D on the plane, $z = 0$, produces a two-dimensional distribution that can be projected (regular Abel transform) to obtain the one-dimensional, projected annihilation density distribution, unaffected by slice thickness

$$P_c(u) = \mathcal{A}\{D(r); u\}$$

$$= \frac{-1}{2\pi}\mathcal{A}\left\{\mathcal{A}_{\sigma_t}\left\{\frac{1}{\sigma_t^2}Q(\rho) - Q'(\rho)/\rho; r\right\}; u\right\}. \qquad (13)$$

Finally, we make use of the Abel transform's commutation and differentiation properties ((A-8) and (A-4) in the Appendix), and the definition of Q to obtain the final expression for P_c as

$$P_c(u) = \frac{-1}{2\pi}\mathcal{A}_{\sigma_t}\left\{\frac{1}{\sigma_t^2}P(u_1) - P'(u_1)/u_1; u\right\} \qquad (14)$$

where u_1 is a dummy variable of integration.

We have employed this expression to correct Derenzo's empirical model for the projected annihilation density distribution function due to ^{11}C. The resulting range distribution curves are shown in the graph of Fig. 2. As would be expected, for radii much greater than the slice thickness there is no difference between the two curves. As r approaches zero however, the difference becomes significant. This calculation demonstrates that the shape of the projected annihilation density distribution arising from a point source depends on the tomographic instrument's slice thickness. Instruments with narrower slices
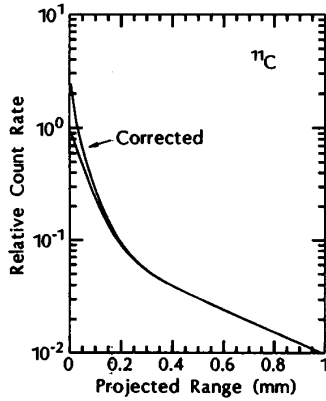
Fig. 2.   Comparison of projected annihilation density distributions, as measured and following correction for slice thickness effects, for a point source of ^{11}C.

will measure projected range distributions due to point sources that are more sharply peaked towards the origin.

B. Line-Spread Functions

A representation of positron range blurring effects which is independent of slice thickness is obtained by considering the two-dimensional line-spread function (LSF), rather than the PSF. This is obtained by taking the forward Abel transform of the three-dimensional point-source distribution,

$$S(\rho) = \mathcal{A}\{D(r); \rho\}. \tag{15}$$

Again we take advantage of the linearity property of the various integral transformations, to express the LSF S in terms of a superposition of range distributions due to projected monoenergetic point sources,

$$S(r) = \int_0^{E_0} Q_m(r; E_i) N(E_i) \, dE_i, \tag{16}$$

with the two-dimensional monoenergetic kernel defined by

$$Q_m(r; E_i) = \frac{1}{2\pi\sigma^2} e^{-r^2/2\sigma^2}. \tag{17}$$

We have calculated LSF's by numerically integrating (16) for six positron emitting isotopes that are of medical interest. There results are shown in the graphs of Fig. 3.

C. Image Resolution Loss

Due to the form of the annihilation density model of (16) it is straight-forward to obtain an expression for the image-plane resolution function which combines the positron range effects and those due to other systematic degradations. Consider now a camera resolution function which is approximately Gaussian in form, with a standard deviation of σ_c. The combined LSF is therefore given by the two-dimensional convolution of these terms, or

$$L_t(r) = L_c(r) \star S(r) \tag{18}$$

where L_t is the combined LSF, L_c the camera's LSF describ-
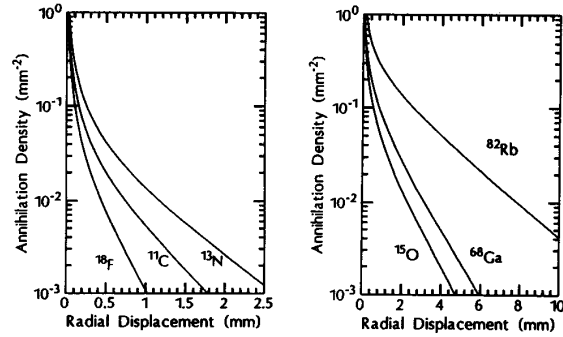

Fig. 3.   Line-spread functions representing annihilation density distributions calculated by Abel transformation of the three-dimensional point source model equation. Resulting distributions due to line sources of six positron emitters are shown.

ing all systematic effects other than positron range, and S is the LSF due to positron range blurring, as given in (16). The resulting expression for the combined effects is

$$L_t(r) = \int_0^{E_0} \frac{1}{2\pi\sigma_e^2} e^{-r^2/2\sigma_e^2} N(E_i) \, dE_i \tag{19}$$

in which a new effective standard deviation σ_e, which is a function of energy E_i has been introduced and is given by

$$\sigma_e = \sqrt{\sigma^2 + \sigma_c^2} \tag{20}$$

where σ_c is the standard deviation which parameterizes the camera's LSF. Although σ_e has the same form as σ_f, introduced earlier, there is an important difference—σ_e incorporates a blurring effect due to the camera's limited in-plane resolution, (σ_c) and σ_f incorporated the blurring effects associated with the slice "thickness" (σ_t).

We have performed calculations based on (19) over a range of beta end-point energies and for three hypothetical isotopes having atomic numbers 10, 25, and 40, respectively. As a reference, we have set the camera LSF to be Gaussian in form, and have calculated combined LSF's for camera resolutions of 1 mm, 2 mm, 4 mm, and 6 mm FWHM. The results for these twelve parameter variations are illustrated in the graphs of Fig. 4 as FWHM and full-width at one tenth maximum (FWTM) values of the combined LSF plotted against isotope end-point energy.

IV. Discussion

We have introduce a model for predicting the annihilation density distribution arising from a point source positron emitter. The model combines the beta-decay energy spectrum and an empirical formula that describes the experimental results of electron beam transmission experiments. We have demonstrated that the model predictions are in close agreement with published data for experimental measurements made on three positron emitters. We have thus used the model to evaluate image-plane line-spread functions due to range effects for a total of six medically important radio-isotopes.

This work has relied on the experimental measurements of Derenzo [7], [5] which we feel are the most accurate to date.
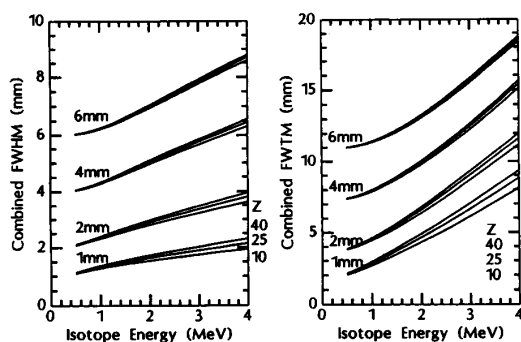
Fig. 4. Model predictions of FWHM (left) and FWTM (right) due to the combined effects of tomograph resolution and positron range. Curves are shown for hypothetical isotopes with three different atomic numbers Z as marked. Detector LSF is assumed to be Gaussian in form, with intrinsic spatial resolution of 1 mm, 2 mm, 4 mm, and 6 mm FWHM, as indicated.

The model presented here produces results which are in close agreement with those experimental data, and can be used to predict annihilation distributions due to positron range effects for any isotope.

Both the experimental technique of Derenzo, and the model introduced here are expected to produce the least reliable results at or near the point of emission—the experiment, because of instrument resolution limitations, and the model because of the assumption that positrons behave diffusively. Indeed we have observed the greatest systematic difference between the two results towards the origin of the projected point-spread functions (see Fig. 1).

As expected, the degree of image resolution loss is strongly dependent on end-point energy. To a lesser degree, but nevertheless significant, we observe a loss of image resolution that is related to the atomic number of the positron emitting isotope. This dependence is not surprising given that the shape of the emission energy spectrum depends on atomic number as well as end-point energy. This result suggests that the blurring effect of an ^{15}O tracer should be less severe than that of ^{68}Ga to a great degree than would be expected from a consideration of end-point energy alone. Indeed Cho et al. [6] have made note of this apparent discrepancy. From our results for a camera resolution of 1 mm FWHM, the combined ^{15}O FWHM is predicted to be 12 percent lower and the FWTM 18 percent lower than the corresponding results for ^{68}Ga although the ^{15}O end-point energy is only 8% lower than that of ^{68}Ga.

In addition to the dependence of these results on atomic number, the graphs of Fig. 4 demonstrate that the nature of the resolution loss depends on the camera resolution. The effects of positron range cannot be estimated by adding in quadrature an approximate blurring parameter to the camera resolution, as would be possible for Gaussian shaped annihilation distributions. It is clear that the most serious resolution degradation is due to the long tails of the distribution and therefore the effects are more apparent in the FWTM than the FWHM results. In addition to this, these results suggest that higher resolution cameras will be less affected by positron range effects, if we consider the loss of resolution as seen in the FWHM measure of the combined LSF curves of Fig. 4. For a camera

possessing a spatial resolution of 3 mm FWHM the positron range effect degrades the resolution by an extra 2 mm for a hypothetical 4 MeV isotope, compared to only 1 mm increase in combined FWHM measurement for the same isotope in a camera possessing 1 mm FWHM spatial resolution.

As the spatial resolution of future positron tomographs improves, the blurring effect of positron range is likely to become more of a concern. While the long tails of the annihilation distribution functions cause a portion of the image to be blurred severely, the sharp peaks, as Derenzo has pointed out, do help to retain high spatial frequency information. This type of degradation is therefore well suited to image restoration schemes [15], that remove the severely blurred image components, operating much like the scatter correction schemes that are in general use in the PET field [16]. The model presented in this work may assist the designers of future high-resolution PET detectors as well as the designers of image postprocessing and restoration schemes.

APPENDIX
ABEL TRANSFORMS

Two integral transformations naturally arise in the analysis of tomographic imaging systems: the Abel transform and a Gaussian weighted variation (referred to here as the *weighted Abel transform*). Both these transformations define mappings between multidimensional symmetric distributions. The forward transforms reduce the dimensionality by one. By symmetry, we mean that the function can be expressed in terms of a single scalar variable which is the Euclidian distance from the coordinate system origin.

A.1 Able Transform

The Abel transform is defined by the integral expression,

$$\mathcal{A}\{f(r); u\} = p(u) = \int_{-\infty}^{\infty} f\left(\sqrt{u^2 + t^2}\right) dt \qquad \text{(A-1)}$$

in which p is any parallel projection of a circularly symmetric function, or the Abel transform of f. The Abel transform has an inverse, which is given by the expression

$$\mathcal{A}^{-1}\{p(u); r\} = f(r) = -\frac{1}{\pi} \int_r^{\infty} \frac{1}{\sqrt{t^2 - r^2}} p'(t) \, dt. \qquad \text{(A-2)}$$

Derivations can be found in [17, p. 406], and [18, p. 262], and a more rigorous mathematical development is presented in [19].

It can be shown by manipulation of these two equations that the forward and inverse Abel transforms are related, i.e.,

$$\mathcal{A}^{-1}\{f(r); u\} = \frac{-1}{2\pi} \mathcal{A}\left\{\frac{1}{r}\frac{df}{dr}; u\right\}. \qquad \text{(A-3)}$$

Furthermore, a simple but very useful expression can be obtained by differentiating the expression for the forward transform, (A-1),

$$\frac{1}{u}\frac{dp}{du} = \mathcal{A}\left\{\frac{1}{r}\frac{df}{dr}; u\right\}. \qquad \text{(A-4)}$$

A.2 Weighted Abel Transform

We define here a variation on the Abel transform, referred to as the weighted Abel transform, that introduces a Gaussian term into the Abel integral. This new transform is defined by

$$\mathcal{A}_\sigma\{f(r); u\} = p_\sigma(u)$$

$$= \int_{-\infty}^{\infty} f\left(\sqrt{u^2 + t^2}\right) e^{-t^2/2\sigma^2} \, dt \quad \text{(A-5)}$$

where the parameter σ is the Gaussian standard deviation. Multiplying this equation by an exponential term, we obtain the relationship between the weighted and regular Abel transform,

$$p_\sigma(u)e^{-u^2/2\sigma^2} = \mathcal{A}\left\{f(r)e^{-r^2/2\sigma^2}; u\right\}. \quad \text{(A-6)}$$

By making use of this relationship, and the equation for the inverse Abel transform, (A-2), we obtain an inversion formula for the weighted Abel transform:

$$\mathcal{A}_\sigma^{-1}\{p_\sigma(u); r\} = \frac{-1}{2\pi} \mathcal{A}_\sigma\left\{\frac{1}{\sigma^2}p_\sigma(u) - \frac{1}{u}\frac{dp_\sigma}{du}; r\right\}. \quad \text{(A-7)}$$

We also note that both transforms, $\mathcal{A}$ and $\mathcal{A}_\sigma$ are linear, and they commute, i.e.,

$$\mathcal{A}\{\mathcal{A}_\sigma\{f(r); u\}; r\} = \mathcal{A}_\sigma\{\mathcal{A}\{f(r); u\}; r\}. \quad \text{(A-8)}$$

ACKNOWLEDGMENT

REFERENCES

[1] S. E. Derenzo, R. H. Huesman, J. L. Cahoon, A. Geyer, D. Uber, T. Vuletich, and T. F. Budinger, "Initial results from the Donner 600 crystal positron tomograph," *IEEE Trans. Nuclear Sci.* vol. NS-34, pp. 321–325, Feb. 1987.

[2] G. L. Brownell, C. A. Burnham, and D. A. Chesler, "High resolution tomograph using analog coding," in *The Metabolism of the Human Brain Studied with Positron Emission Tomography*, T. Greitz *et al.*, Eds. New York: Raven, 1985, pp. 13–19.

[3] P. Colombino, B. Fiscella, and L. Trossi, "Study of positronium in water and ice from 22 to −144°C by annihilation quanta measurements," *Nuovo Cimento*, vol. 38, no. 2, pp. 707–725, 1965.

[4] H. Iida, I. Kanno, S. Miura, M. Murakami, K. Takahashi, and K. Uemura, "A simulation study of a method to reduce positron annihilation spread distributions using a strong magnetic field in positron emission tomograph," *IEEE Trans. Nuclear Sci.*, vol. NS-33, pp. 597–600, Feb. 1986.

[5] S. E. Derenzo, "Mathematical removal of positron range blurring in high resolution tomography," *IEEE Trans. Nuclear Sci.*, vol. NS-33, pp. 546–549, 1986.

[6] Z. H. Cho, J. K. Chan, L. Ericksson, M. Singh, S. Graham, N. S. Macdonald, and Y. Yano, "Positron ranges obtained from biomedically important positron-emitting radionuclides," *J. Nuclear Med.*, vol. 16, pp. 1174–1176, 1975.

[7] S. E. Derenzo, "Precision measurement of annihilation point spread distributions for medicaly important positron emitters," in *Positron Annihilation* R. R. Hasiguti and K. Fujiwara, Eds. Sendai, Japan: The Japan Institute of Metals, 1979, pp. 819–823.

[8] M. E. Phelps, E. J. Hoffman, and S. Huang, "Effects of positron range on spatial resolution," *J. Nuclear Med.*, vol. 16, no. 7, pp. 649–652, 1975.

[9] A. Nelm, "Energy loss and range of electrons and positrons," Tech. Rep. Circular 577, NBS, 1956.

[10] W. Heitler, *The Quantum Theory of Radiation*. New York: Dover, 1953. (Originally published: 3rd ed. Oxford: Clarendon Press, 1954).

[11] R. D. Evans, *The Atomic Nucleus*. New York: McGraw-Hill, 1955.

[12] T. Tabata, R. Ito, and S. Okagbe, "Generalized semiempirical equations for the extrapolated range of electrons," *Nuclear Instrument. Meth.*, vol. 103, pp. 85–91, 1972.

[13] N. Tsoulfanidis, *Measurement and Detection of Radiation*. New York: Hemisphere, 1983.

[14] F. Rohrlich and B. C. Carlson, "Positron-electron differences in energy loss and multiple scattering," *Phys. Rev.*, vol. 93, p. 38, 1954.

[15] A. Rosenfeld and A. C. Kak, *Digital Picture Processing*. New York: Academic, 1982, 2nd ed.

[16] M. Bergstrom, L. Eriksson, C. Bohm, G. Blomqvist, and J. Litton, "Correction for scattered radiation in a ring detector positron camera by integral transformation of the projections," *J. Comut. Assist. Tomography*, vol. 7, pp. 42–50, 1983.

[17] H. H. Barrett and W. Swindell, *Radiological Imaging*. New York: Academic, 1981, vols. 1 and 2.

[18] R. N. Bracewell, *The Fourier Transform and Its Applications*. New York: McGraw-Hill, 1986, 2nd ed.

[19] F. Natterer, *The Mathematics of Computerized Tomography*. New York: Wiley, 1986.